A matrix inversion approach of computing T-matrix for axially symmetrical particles of extreme shape and dielectrically large dimension

Xinyi Shen,[1,2] Qiming Qin,[1] Yang Hong,[2,3] and Guifu Zhang[3,4]

Received 30 October 2011; revised 11 July 2012; accepted 24 July 2012; published 18 September 2012.

[1] The T-matrix method has been widely used in radar meteorology because hydrometeors approximate to spheroidal shapes and their sizes are comparable to the sensing wavelength. However, it is considered unsuitable to solve in remote sensing problems concerning vegetation because the particles of interest, leaves and branches, are considered extremely shaped and of large dielectric dimensions, therefore beyond the domain of direct T-matrix algorithms. By solving two linear equation sets, this paper proposes a matrix inversion approach to calculate indirectly the T-matrix of regularly shaped scatterers in the crown layer of canopies. We adopt an existing electromagnetic (EM) model to calculate the scattering amplitudes as the left hand side of the equations. The number of the unknowns in the equations decreases by almost half, thus reducing the kernel computation to a significant extent when we assume that the particles are symmetrical in most remote sensing applications. The observed consistency between the scattering coefficients computed by the obtained T-matrix and those by the EM model indicates that the valid aspect ratio of this proposed method spans from 0.02 to 200, although this ratio may possibly extend with further verification. The proposed T-matrix calculation method can work at either the far-zone or the near-zone. However, it should be noted that the T-matrix obtained in the far-zone could not yield correct scattering results in the near-zone; on the contrary, the T-matrix obtained from the near-zone can produce accurate scattering fields/coefficients in what is further than the region of matching.

Citation: Shen, X., Q. Qin, Y. Hong, and G. Zhang (2012), A matrix inversion approach of computing T-matrix for axially symmetrical particles of extreme shape and dielectrically large dimension, *Radio Sci.*, *47*, RS5005, doi:10.1029/2011RS004906.

1. Introduction

[2] The significance of canopy scattering cannot be overstated in remote sensing, water resources management or hydrologic modeling. The canopy consists of leaves and branches that are randomly oriented and distributed. The leaves are usually approximated by oblate cylinders (circular disks) [*Eom and Fung*, 1984] while the branches are approximated by prolate dielectric cylinders. [*Bracaglia et al.*, 1995; *Eom and Fung*, 1986; *Tsang et al.*, 1981]. Prevailing vegetation scattering models based on vectorized radiative theory (VRT) [*Chandrasekhar*, 1950; *Ishimaru*, 1999] compute the scattering of the crown layer either by using the Generalized Rayleigh-Gans (GRG) [*Eom and Fung*, 1984; *Karam et al.*, 1988] approximation at the low frequency or by the Physical Optical (PO) approximation at the high frequency [*LeVine et al.*, 1983; *Michaeli*, 1984; *Ufimtsev*, 1957]. The total scattering phase function of the crown layer is usually approximated by averaging the intensity of differently oriented scatterers incoherently. This means that 1) the scattering model has to be run repeatedly over multiple discrete orientations, and 2) interactions between the particles in the crown or a sub layer are excluded. The VRT-based canopy scattering models such as MIMICS [*Ulaby et al.*, 1987], KARAM and Matrix Doubling [*Fung*, 1994; *Ulaby et al.*, 1986], improve the precision of simulation significantly by taking the canopy's crown-trunk-ground structure into account. However, the cross-polarized responses tend to be underestimated [*Shen et al.*, 2010] because the contribution of multiple scattering within a sub-layer is neglected.

[3] The numerical algorithms [*Harrington*, 1987; *Tsang et al.*, 1992; *Yee*, 1966; *Zhang et al.*, 1996] provide better accuracy by solving Maxwell's equations without making any approximation. However, these algorithms are not set to calculate the scattering of the vegetation layer that contains thousands of scatterers over a vast range of statistical parameters in remote sensing applications.

[1]Institute of Remote Sensing and GIS, Peking University, Beijing, China.
[2]School of Civil Engineering and Environmental Sciences, University of Oklahoma, Norman, Oklahoma, USA.
[3]Atmospheric Radar Research Center, University of Oklahoma, Norman, Oklahoma, USA.
[4]School of Meteorology, University of Oklahoma, Norman, Oklahoma, USA.

Corresponding author: Q. Qin, Institute of Remote Sensing and GIS, Peking University, Beijing 100871, China. (qmqin@pku.edu.cn)

0048-6604/12/2011RS004906

[4] The matrix formulation of the scattering problem, referred to as the transfer matrix (T-matrix), has been elaborated [*Mishchenko*, 1990, 1991, 1993; *Mishchenko*, 2000; *Mishchenko and Travis*, 1998; *Mishchenko et al.*, 2005; *Oguchi*, 1981] for more than three decades since it was initially proposed [*Waterman*, 1965]. Most of these advances have been thoroughly discussed by *Mishchenko et al.* [1996]. The T-matrix solution dominates the scattering problem in radar meteorology because it helps quickly obtain the scattering coefficients of arbitrary directions of the incidence, scattering and particle orientation once the T-matrix of the particle is calculated. Moreover, the T-matrix is an exact solution of Maxwell's equation [*Waterman*, 1965] thus yielding better accuracy than GRG or PO in the intersection of their valid region. In addition, the most attractive property of the T-matrix is its capability to take the entire multiple scattering from a cluster of particles into consideration by employing the Foldy-Lax approximation [*Foldy*, 1945; *Lax*, 1951]. The Foldy-Lax approximation traces the interactions between scatterers by superimposing the scattered waves to the incidence. The Foldy-Lax approximation was solved initially by the iterative method [*Tsang et al.*, 2001] and was later solved with better accuracy using the cluster T-matrix approach to calculate densely distributed spheres [*Lu et al.*, 1993; *Mackowski*, 1994; *Mishchenko et al.*, 1996; *Tsang et al.*, 2001; *Wang and Chew*, 1993]. The advantages of the cluster T-matrix version make it a viable candidate for solving the scattering problem of the crown layer.

[5] Despite the potential of applying the T-matrix to vegetation remote sensing, the inability to handle large dimensions and extreme shapes whose aspect ratio, the ratio of the radius to the half-length, is far from unity [*Mishchenko*, 1993; *Mishchenko and Travis*, 1998; *Mishchenko et al.*, 1996] prevents the T-matrix method from being widely used in this field. The currently available T-matrix codes require numerical integration of Bessel and Hankel functions over the surface of the particle in its kernel step. Unfortunately, Bessel functions $j_n(k_s r)$ oscillate quickly with respect to the radius, r [*Tsang et al.*, 2000]. When the wave number k_s is a complex in a lossy medium, the order in magnitude of $j_n(k_s r)$ grows rapidly when r increases. Meanwhile, the Hankel function $h_n(kr)$ increases sharply when r approaches the origin, where k is the wave number of the free space. In case of extreme shapes, the integral with respect to r does not often converge over a wide range. Moreover, even if the integration can be calculated accurately, the matrix that requires inversion is usually singular, especially at highly truncated orders, which is the case of extreme shaped particles. Some studies [*Iskander and Lakhtakia*, 1984; *Lakhtakia et al.*, 1983; *Yan et al.*, 2009] employed the iterative extended boundary condition method (IEBCM) to solve the scattering of extreme shaped particles by dividing them into sub-objects and matching the extended boundary condition iteratively. However, such a strategy does not apply to high-loss dielectric objects [*Iskander and Lakhtakia*, 1984] and incurs substantial changes to the T-matrix algorithm thus increasing the complexity [*Mishchenko et al.*, 1996] of the code significantly. Meanwhile the IEBCM does not include the oblate particle type. *Lakhtakia et al.* [1984] indicates that a modified Gram-Schmidt reinforced orthogonalization can circumvent inverting the singular matrix numerically for the lossless particle. The recursive T-matrix method [*Gürel and Chew*, 1992; *Wang and Chew*, 1992, 1993] combines the MOM and T-matrix to solve the scattering of a 2-D thin conductor. It requires great knowledge of the workflow of MOM in order to recur to the current distribution step in MOM, and also limits the valid region of the recursive T-matrix to that of MOM. The Point Matching Method (PMM) of the T-matrix was initially proposed by *Nieminen et al.* [2003] for optical traps. By using data of the extended precision instead of the double precision [*Mishchenko and Travis*, 1998; *Mishchenko et al.*, 1996], the T-matrix works for aspect ratios as large as 20 according to [*Mishchenko et al.*, 1996]. Such aspect ratios meet the range of hydrometeors such as aerosols, raindrops and even dry snow, but not leaves and branches. Typical dry snow has an aspect ratio of 6, whereas that of a 5-cm radius leaf may reach 200. Additionally, since the T-matrix is unable to handle the opposite extreme, i.e., aspect ratios smaller than unity by several orders of magnitude, it is not an adequate solution to branches. Finally, compared to atmospheric particles, scatterers in canopies are dielectrically too large to make the T-matrix practical.

[6] To utilize the advantages of the T-matrix to calculate the canopy scattering, this paper proposes a matrix inversion approach that circumvents its limitation on extreme shapes. Instead of calculating the T-matrix elements directly, this approach obtains the T-matrix elements by solving two linear sets of equations that use the scattering amplitudes calculated by an existing electromagnetic (EM) model. This paper is organized in the following order. Section 2 derives the formulae of the proposed approach. The basic definition of the original T-matrix theory is introduced in Section 2.1 for ease of reference. In Section 2.2, we obtain the kernel formulae of this work as well as describe the computational steps. In Section 3, some numerical issues are discussed, followed by a description of the EM model. We then compare the scattering results of the extreme shapes calculated by the proposed method and the employed EM model. The limitation of the proposed method is analyzed at the end of Section 3. The T-matrix discussed in this paper involves only the traditional localized source (LS) type. In the framework of the LS T-matrix, all the spherical harmonics have one origin that is usually the geometric center of the particle. Therefore, the valid region of the LS T-matrix corresponds to the proposed method, which is outside of the minimum circumscribing sphere of the scatterer.

2. The Matrix Inversion Approach

2.1. The Basic Definition of T-Matrix

[7] In spherical coordinates, a plane incident wave can be expanded using spherical harmonics [*Stratton*, 1941] as in equation (1). The time factor, $e^{-j\omega t}$, is suppressed throughout this paper.

$$\vec{E}^{inc}(\vec{r}\,') = \sum_{n=-\infty}^{\infty}\sum_{m=-n}^{n}\Big[a_{mn}(\theta',\varphi')Rg\vec{M}_{mn}(k\vec{r}\,') + b_{mn}(\theta',\varphi')Rg\vec{N}_{mn}(k\vec{r}\,')\Big] \quad (1)$$

where $Rg\vec{M}_{mn}$, $Rg\vec{N}_{mn}$ are the spherical harmonics that are regular at the origin and infinity, obeying the vector wave equation [*Stratton*, 1941] i.e.,

$$\nabla \times \nabla \times Rg\vec{M}_{mn} - k^2 Rg\vec{M}_{mn} = 0 \tag{2}$$

$$\nabla \times \nabla \times Rg\vec{N}_{mn} - k^2 Rg\vec{N}_{mn} = 0 \tag{3}$$

The complete form of the coefficients, a_{mn}, b_{mn} and the spherical harmonics, $Rg\vec{M}_{mn}$ and $Rg\vec{N}_{mn}$ are in equations (A1)–(A12) in Appendix A.

[8] The scattered wave, however, can be expanded in equation (4) using the outgoing harmonics which satisfy the radiation condition thus decaying to zero at infinity and is infinite at the origin [*Waterman*, 1965].

$$\vec{E}^{\,\mathrm{sca}}(\vec{r}) = \sum_{n=-\infty}^{\infty} \sum_{m=-n}^{n} \left[p_{mn} \vec{M}_{mn}(k\vec{r}) + q_{mn} \vec{N}_{mn}(k\vec{r}) \right] \tag{4}$$

The expressions of $\vec{M}_{mn}(\vec{r})$ and $\vec{N}_{mn}(\vec{r})$ are respectively the same as $Rg\vec{M}_{mn}(\vec{r})$ and $Rg\vec{N}_{mn}(\vec{r})$ with the first kind of spherical Bessel function replaced by the first kind of spherical Hankel function. Since the spherical harmonics are known functions, the incident and scattered waves can be represented by their coefficient vectors, i.e., $\begin{bmatrix} \boldsymbol{a}_{m'n'} \\ \boldsymbol{b}_{m'n'} \end{bmatrix}$ and $\begin{bmatrix} \boldsymbol{p}_{mn} \\ \boldsymbol{q}_{mn} \end{bmatrix}$. The T-matrix [*Waterman*, 1965] transfers the coefficients of incidence to the scattered coefficients in equation (5) . Then the scattered coefficients are substituted into equation (4) to get the scattering amplitudes.

$$\begin{bmatrix} \boldsymbol{p}_{mn} \\ \boldsymbol{q}_{mn} \end{bmatrix} = \overline{\overline{\boldsymbol{T}}} \begin{bmatrix} \boldsymbol{a}_{m'n'} \\ \boldsymbol{b}_{m'n'} \end{bmatrix} \tag{5}$$

For axially symmetrical particles, the T-matrix elements become zero unless $m = m'$ [*Waterman*, 1965], i.e.,

$$T_{mnm'n'} = T_{mnn'} = \delta_{mm'} T_{mnm'n'} \tag{6}$$

Therefore, the T-matrix can be regrouped according to the m-index in order to form a block-diagonal matrix. In practice, the infinite n has to be truncated to $n_{\max}$. There is a total of $2n_{\max} + 1$ blocks. Each block can be written as

$$\overline{\overline{\boldsymbol{T}}}_{\boldsymbol{m}} = \begin{bmatrix} \overline{\overline{\boldsymbol{T}}}^{11}_{\boldsymbol{mnn'}} & \overline{\overline{\boldsymbol{T}}}^{12}_{\boldsymbol{mnn'}} \\ \overline{\overline{\boldsymbol{T}}}^{21}_{\boldsymbol{mnn'}} & \overline{\overline{\boldsymbol{T}}}^{22}_{\boldsymbol{mn'n'}} \end{bmatrix}, \boldsymbol{m} \le \boldsymbol{n}, \boldsymbol{n'} \le \boldsymbol{n}_{max} \tag{7}$$

2.2. The Matrix Inversion Procedure

[9] As mentioned in section 1, the T-matrix depends solely on the shape, dielectric and orientation of a particle. Since the T-matrix of the non-oriented (z axis is the rotational axis of the particle) particle can be easily transformed [*Mishchenko*, 1991; *Mishchenko et al.*, 1996] to the T-matrix of an arbitrary oriented particle, we consider only the T-matrix of the non-oriented particle in the scope of this study. From equation (5), we conclude that the scattered coefficient vector $\begin{bmatrix} \boldsymbol{p}_{mn} \\ \boldsymbol{q}_{mn} \end{bmatrix}$ depends exclusively on the incident wave and the particle. Meanwhile $\begin{bmatrix} \boldsymbol{p}_{mn} \\ \boldsymbol{q}_{mn} \end{bmatrix}$ is equivalent to the surface current distribution excited by the incident wave [*Barber and Yeh*, 1975]. Therefore, for a given particle, each incidence produces a scattered coefficient vector. The proposed method can be summarized into four steps: 1) fix one incident wave and calculate the scattered fields in multiple directions and all polarizations using the existing EM model, 2) use the scattered fields to obtain the scattered coefficient vector $\begin{bmatrix} \boldsymbol{p}_{mn} \\ \boldsymbol{q}_{mn} \end{bmatrix}$ for the given incidence and particle, 3) change the direction and polarization of the incidence to repeat steps 1) and 2) to get adequate coefficient vectors, 4) use the incidence and scattered coefficient vector to inversely get the T-matrix elements block by block. The four steps above are described in detail in the following subsections.

2.2.1. Matching the Scattered Coefficient Vector Using the Existing EM Model

[10] The scattered coefficient vector $\begin{bmatrix} \boldsymbol{p}_{mn} \\ \boldsymbol{q}_{mn} \end{bmatrix}$ can be solved for at either the far-zone which is infinity or the near-zone which is the finite region starting from the surface of the particle. However, the valid scattered field expansion of the LS T-matrix proves to be outside of the minimum circumscribing sphere of the particle [*Waterman*, 1965]. We have discussed this limitation in section 3.3 and narrowed down the near–zone to the region between the minimum circumscribing sphere and infinity in the scope of this study.

2.2.1.1. Matching At Far-Zone

[11] The Sinclair matrix [*Lee and Pottier*, 2009; *Mishchenko et al.*, 2005] is defined in equation (8)

$$\begin{bmatrix} E^{sca}_{\theta}(\vec{r}) \\ E^{sca}_{\varphi}(\vec{r}) \end{bmatrix} = \frac{e^{ikr}}{r} \overline{\overline{S}}(\hat{n}^{sca}, \hat{n}^{inc}) \cdot \begin{bmatrix} E^{inc}_{0\theta} \\ E^{inc}_{0\varphi} \end{bmatrix} \tag{8}$$

where

$$\overline{\overline{S}}(\hat{n}^{sca}, \hat{n}^{inc}) = \begin{bmatrix} S_{\theta\theta} & S_{\theta\varphi} \\ S_{\varphi\theta} & S_{\varphi\varphi} \end{bmatrix} \tag{9}$$

Applying the far-zone limit, i.e.

$$\lim_{r\to\infty} \vec{M}_{mn}(kr, \theta, \varphi) = \frac{(-1)^m (-i)^{n+1} e^{ikr}}{kr} d_n \vec{C}_{mn}(\theta) e^{im\varphi} \tag{10}$$

$$\lim_{r\to\infty} \vec{N}_{mn}(kr, \theta, \varphi) = \frac{(-1)^m (-i)^{n} e^{ikr}}{kr} d_n \vec{B}_{mn}(\theta) e^{im\varphi} \tag{11}$$

of the outgoing harmonics in equations (4) and (8), where d_n is the order related coefficient given in equation (A12) while $\vec{B}_{mn}(\theta)$ and $\vec{C}_{mn}(\theta)$ are the Associated Legendre function related factors given in equations (A7) and (A8), we obtain the expression of the far-zone field which is usually used to calculate the radar cross section,

$$\begin{aligned} \frac{e^{ikr}}{r} \overline{\overline{S}} \cdot \vec{E}^{\,inc} = \vec{E}^{\,\mathrm{sca}}(\vec{r}) &= \sum_{n=-\infty}^{\infty} \sum_{m=-n}^{n} \left[p_{mn} \vec{M}_{mn}(\vec{r}) + q_{mn} \vec{N}_{mn}(\vec{r}) \right] \\ &= \sum_{n=-\infty}^{\infty} \sum_{m=-n}^{n} \left[p_{mn} \frac{(-1)^m (-i)^{n+1} e^{ikr}}{kr} d_n \vec{C}_{mn}(\theta) e^{im\varphi} \right. \\ &\quad \left. + q_{mn} \frac{(-1)^m (-i)^{n} e^{ikr}}{kr} d_n \vec{B}_{mn}(\theta) e^{im\varphi} \right] \end{aligned} \tag{12}$$

Cancelling the $\frac{e^{ikr}}{r}$ on both sides of equation (12), we obtain

$$\overline{\overline{S}} \cdot \vec{E}^{inc} = \frac{1}{k} \sum_{n=-\infty}^{\infty} \sum_{m=-n}^{n} \left[p_{mn}(-1)^m (-i)^{n+1} d_n \vec{C}_{mn}(\theta) e^{im\varphi} + q_{mn}(-1)^m (-i)^n d_n \vec{B}_{mn}(\theta) e^{im\varphi} \right] \quad (13)$$

We use equation (13) to compute $\begin{bmatrix} \boldsymbol{p_{mn}} \\ \boldsymbol{q_{mn}} \end{bmatrix}$ when we get the Sinclair matrices of adequate discrete scattered directions excited by a given incidence. Equation (13) at multiple scattering angles and polarizations composes a linear equation-set. Taking advantage of the axially symmetrical property of the particle, we get the relationship between $\begin{bmatrix} \boldsymbol{p_{mn}} \\ \boldsymbol{q_{mn}} \end{bmatrix}$ and $\begin{bmatrix} \boldsymbol{p_{-mn}} \\ \boldsymbol{q_{-mn}} \end{bmatrix}$ in equations (14)–(17), which helps minimize the number of unknowns. At $\hat{\varphi}$ polarized incidence, we have

$$p_{-mn} = (-1)^m p_{mn} \quad (14)$$

$$q_{-mn} = (-1)^{m+1} q_{mn} \quad (15)$$

At $\hat{\theta}$ polarized incidence, we have

$$p_{-mn} = (-1)^{m+1} p_{mn} \quad (16)$$

$$q_{-mn} = (-1)^m q_{mn} \quad (17)$$

The proof of equations (14)–(17) is given in detail in Appendix A through equations (A13)–(A20). From equations (14)–(17), we need to solve exclusively for the scattered coefficient vector of positive m subscript. Therefore, the number of the unknowns is reduced by half. The terms where $m = 0$ in equation (13) are written as

$$\sum_{m=0} = \sum_{n=-\infty}^{\infty} f_{01} \vec{C}_{0n}(\theta) p_{0n} + f_{02} \vec{B}_{0n}(\theta) q_{0n} \quad (18)$$

where

$$f_{01} = (-i)^{n-1} d_n \text{ and } f_{02} = (-i)^n d_n. \quad (19)$$

[12] For the terms where $m \neq 0$ in equation (13), we merge the negative m into its positive correspondence, using equations (14)–(17). We have at $\hat{\varphi}$ polarized incidence

$$\sum_{m>0,\hat{\varphi}} = \sum_{n=1}^{\infty} \sum_{m=1}^{n} 2(-1)^m (-i)^{n+1} d_n Re\left\langle \vec{C}_{mn}(\theta) e^{im\varphi} \right\rangle p_{mn} + 2(-1)^m (-i)^{n-1} d_n Im\left\langle \vec{B}_{mn}(\theta) e^{im\varphi} \right\rangle q_{mn}, m = 1, 2, \ldots, n_{\max} \quad (20)$$

Taking the dot products with $\hat{\varphi}$ and $\hat{\theta}$ respectively at both sides of equation (20), we have the elements of the coefficient matrix for $\hat{\varphi}\hat{\varphi}$ *and* $\hat{\theta}\hat{\varphi}$ responses respectively

$$\sum_{m>0,\hat{\varphi}\hat{\varphi}} = \sum_{n=1}^{\infty} \sum_{m=1}^{n} f_{mn}^{11} [\tau_{mn}(\theta) \cos(m\varphi) p_{mn} + \pi_{mn}(\theta) \cos(m\varphi) q_{mn}] \quad (21)$$

where

$$f_{mn}^{11} = 2(-1)^m (-i)^{n-1} d_n \quad (22)$$

and

$$\sum_{m>0,\hat{\theta}\hat{\varphi}} = \sum_{n=0}^{\infty} \sum_{m=1}^{n} f_{mn}^{21} [\pi_{mn}(\theta) \sin(m\varphi) p_{mn} + \tau_{mn}(\theta) \sin(m\varphi) q_{mn}] \quad (23)$$

where

$$f_{mn}^{21} = f_{mn}^{11} \quad (24)$$

We have similar equations at $\hat{\theta}$ incidence with f_{mn}^{11} and f_{mn}^{21} replaced by f_{mn}^{12} and f_{mn}^{22} respectively, where

$$f_{mn}^{12} = 2(-1)^{m+1} (-i)^n d_n \text{ and } f_{mn}^{22} = 2(-1)^m (-i)^n d_n \quad (25)$$

We know that

$$T_{0nn'}^{ij} = 0, i \neq j \quad (26)$$

From equations (A1) and (A2), we know that $b_{0n} = 0$ at $\hat{\varphi}$ polarization and $a_{0n} = 0$ at $\hat{\theta}$ polarization. Taking equation (5) into consideration, we have

$$p_{0n} = 0, \hat{\theta} \textbf{ polarized incidence} \quad (27)$$

$$q_{0n} = 0, \hat{\varphi} \textbf{ polarized incidence} \quad (28)$$

Using (27) and (28), we can remove the zero rows from $\begin{bmatrix} \boldsymbol{p_{mn}}(\theta_i, \hat{\varphi}) \\ \boldsymbol{q_{mn}}(\theta_i, \hat{\varphi}) \end{bmatrix}$ to decrease the number of the unknowns from $n_{\max}(n_{\max} + 3)$ to $n_{\max}(n_{\max} + 2)$.

[13] Supposing we have employed n_{Ds} discrete scattering angles, equation (13) can be written in the matrix form below in the fully polarimetric manner

$$\begin{bmatrix} \boldsymbol{S_{\hat{\varphi}\hat{p}}}(\boldsymbol{\theta_s}, \theta_i) \\ \boldsymbol{S_{\hat{\theta}\hat{p}}}(\boldsymbol{\theta_s}, \theta_i) \end{bmatrix} = \overline{\overline{\boldsymbol{C}}}_{\hat{p}}^{\boldsymbol{scat}} \begin{bmatrix} \boldsymbol{p_{mn}}(\theta_i, \hat{p}) \\ \boldsymbol{q_{mn}}(\theta_i, \hat{p}) \end{bmatrix}, p = \theta, \varphi \quad (29)$$

where

$$\overline{\overline{\boldsymbol{C}}}_{\hat{p}}^{scat}(n_{Ds}) = \begin{bmatrix} \overline{\overline{\boldsymbol{C}}}_{\hat{\varphi}\hat{p}}^{scat}(n_{Ds}) \\ \overline{\overline{\boldsymbol{C}}}_{\hat{\theta}\hat{p}}^{scat}(n_{Ds}) \end{bmatrix} \quad (30)$$

where

$$\overline{\overline{C}}^{scat}_{\hat{\varphi}\hat{\varphi}}(n_{Ds}) = \frac{1}{k}\begin{bmatrix} \overbrace{\begin{matrix} f_{0n}^{01}\tau_{0n}(\theta_1) & f_{mn}^{11}\tau_{mn}(\theta_1)\cos(m\varphi_1) \\ f_{0n}^{01}\tau_{0n}(\theta_2) & f_{mn}^{11}\tau_{mn}(\theta_2)\cos(m\varphi_2) \\ \vdots & \\ f_{0n}^{01}\tau_{0n}(\theta_{n_{Ds}}) & f_{mn}^{11}\tau_{mn}(\theta_{n_{Ds}})\cos(m\varphi_{n_{Ds}}) \end{matrix}}^{p_{mn}} & \overbrace{\begin{matrix} f_{mn}^{11}\pi_{mn}(\theta_1)\cos(m\varphi_1) \\ f_{mn}^{11}\pi_{mn}(\theta_2)\cos(\varphi m_2) \\ \vdots \\ f_{mn}^{11}\pi_{mn}(\theta_{n_{Ds}})\cos(m\varphi_{n_{Ds}}) \end{matrix}}^{q_{mn}} \end{bmatrix} \tag{31}$$

$$\overline{\overline{C}}^{scat}_{\hat{\theta}\hat{\varphi}}(n_{Ds}) = \frac{1}{k}\begin{bmatrix} \overbrace{\begin{matrix} 0 & f_{mn}^{21}\pi_{mn}(\theta_1)\sin(m\varphi_1) \\ 0 & f_{mn}^{21}\pi_{mn}(\theta_2)\sin(m\varphi_2) \\ & \vdots \\ 0 & f_{mn}^{21}\pi_{mn}(\theta_{n_{Ds}})\sin(m\varphi_{n_{Ds}}) \end{matrix}}^{p_{mn}} & \overbrace{\begin{matrix} f_{mn}^{21}\tau_{mn}(\theta_1)\sin(m\varphi_1) \\ f_{mn}^{21}\tau_{mn}(\theta_2)\sin(m\varphi_2) \\ \vdots \\ f_{mn}^{21}\tau_{mn}(\theta_{n_{Ds}})\sin(m\varphi_{n_{Ds}}) \end{matrix}}^{q_{mn}} \end{bmatrix} \tag{32}$$

$$\overline{\overline{C}}^{scat}_{\hat{\varphi}\hat{\theta}}(n_{Ds}) = \frac{1}{k}\begin{bmatrix} \overbrace{\begin{matrix} f_{mn}^{12}\tau_{mn}(\theta_1)\sin(m\varphi_1) \\ f_{mn}^{12}\tau_{mn}(\theta_2)\sin(m\varphi_2) \\ \vdots \\ f_{mn}^{12}\tau_{mn}(\theta_{n_{Ds}})\sin(m\varphi_{n_{Ds}}) \end{matrix}}^{p_{mn}} & \overbrace{\begin{matrix} 0 & f_{mn}^{12}\pi_{mn}(\theta_1)\sin(m\varphi_1) \\ 0 & f_{mn}^{12}\pi_{mn}(\theta_2)\sin(m\varphi_2) \\ & \vdots \\ 0 & f_{mn}^{12}\pi_{mn}(\theta_{n_{Ds}})\sin(m\varphi_{n_{Ds}}) \end{matrix}}^{q_{mn}} \end{bmatrix} \tag{33}$$

$$\overline{\overline{C}}^{scat}_{\hat{\theta}\hat{\theta}}(n_{Ds}) = \frac{1}{k}\begin{bmatrix} \overbrace{\begin{matrix} f_{mn}^{22}\pi_{mn}(\theta_1)\cos(m\varphi_1) \\ f_{mn}^{22}\pi_{mn}(\theta_2)\cos(m\varphi_2) \\ \vdots \\ f_{mn}^{22}\pi_{mn}(\theta_{n_{Ds}})\cos(m\varphi_{n_{Ds}}) \end{matrix}}^{p_{mn}} & \overbrace{\begin{matrix} f_{mn}^{22}\tau_{mn}(\theta_1)\cos(m\varphi_1) \\ f_{mn}^{22}\tau_{mn}(\theta_2)\cos(m\varphi_2) \\ \vdots \\ f_{mn}^{22}\tau_{mn}(\theta_{n_{Ds}})\cos(m\varphi_{n_{Ds}}) \end{matrix}}^{q_{mn}} \end{bmatrix} \tag{34}$$

where $1 \le m \le n$ throughout equations (31)–(34).

2.2.1.2. Matching At Near-Zone

[14] In the near-zone, we employ the scattered field instead of the Sinclair matrix, meaning that the phase factor by distance and the amplitude decay have been accounted for. Meanwhile, in spherical coordinates, the scattered field component at the radius direction is not zero. Following the same flow, we have a similar linear equation-set to calculate $\begin{bmatrix} \boldsymbol{p_{mn}} \\ \boldsymbol{q_{mn}} \end{bmatrix}$, which is written

$$\begin{bmatrix} \boldsymbol{S}_{\hat{\varphi}\hat{p}}(\theta_s,\theta_i) \\ \boldsymbol{S}_{\hat{\theta}\hat{p}}(\theta_s,\theta_i) \\ \boldsymbol{S}_{\hat{r}\hat{p}}(\theta_s,\theta_i) \end{bmatrix} = \overline{\overline{\boldsymbol{C}}}^{scat}_{\hat{p}} \begin{bmatrix} \boldsymbol{p_{mn}}(\theta_i,\hat{p}) \\ \boldsymbol{q_{mn}}(\theta_i,\hat{p}) \end{bmatrix}, p = \theta, \varphi \tag{35}$$

where

$$\overline{\overline{\boldsymbol{C}}}^{scat}_{\hat{p}} = \begin{bmatrix} \overline{\overline{\boldsymbol{C}}}^{scat}_{\hat{\varphi}\hat{p}}(n_{Ds1}) \\ \overline{\overline{\boldsymbol{C}}}^{scat}_{\hat{\theta}\hat{p}}(n_{Ds2}) \\ \overline{\overline{\boldsymbol{C}}}^{scat}_{\hat{r}\hat{p}}(n_{Ds3}) \end{bmatrix} \tag{36}$$

At $\hat{\varphi}$ incidence

$$\overline{\overline{C}}^{scat}_{\hat{\varphi}\hat{\varphi}}(n_{Ds}) = \begin{bmatrix} \overbrace{\begin{matrix} \frac{1}{2}f_{0n}^{11}(r_1)\tau_{0n}(\theta_1) & f_{mn}^{11}(r_1)\tau_{mn}(\theta_1)\cos(m\varphi_1) \\ \frac{1}{2}f_{0n}^{11}(r_2)\tau_{0n}(\theta_2) & f_{mn}^{11}(r_2)\tau_{mn}(\theta_2)\cos(m\varphi_2) \\ & \vdots \\ \frac{1}{2}f_{0n}^{11}(r_{n_{Ds}})\tau_{0n}(\theta_{n_{Ds}}) & f_{mn}^{11}(r_{n_{Ds}})\tau_{mn}(\theta_{n_{Ds}})\cos(m\varphi_{n_{Ds}}) \end{matrix}}^{p_{mn}} & \overbrace{\begin{matrix} f_{mn}^{21}(r_1)\pi_{mn}(\theta_1)\cos(m\varphi_1) \\ f_{mn}^{21}(r_2)\pi_{mn}(\theta_2)\cos(m\varphi_2) \\ \vdots \\ f_{mn}^{21}(r_{n_{Ds}})\pi_{mn}(\theta_{n_{Ds}})\cos(m\varphi_{n_{Ds}}) \end{matrix}}^{q_{mn}} \end{bmatrix} \tag{37}$$

$$\overline{\overline{C}}^{scat}_{\hat{\theta}\hat{\varphi}}(n_{Ds}) = \begin{bmatrix} \overbrace{\begin{matrix} 0 & f_{mn}^{11}(r_1)\pi_{mn}(\theta_1)\sin(m\varphi_1) \\ 0 & f_{mn}^{11}(r_2)\pi_{mn}(\theta_2)\sin(m\varphi_2) \\ & \vdots \\ 0 & f_{mn}^{11}(r_{n_{Ds}})\pi_{mn}(\theta_{n_{Ds}})\sin(m\varphi_{n_{Ds}}) \end{matrix}}^{p_{mn}} & \overbrace{\begin{matrix} f_{mn}^{21}(r_1)\tau_{mn}(\theta_1)\sin(m\varphi_1) \\ f_{mn}^{21}(r_2)\tau_{mn}(\theta_2)\sin(m\varphi_2) \\ \vdots \\ f_{mn}^{21}(r_{n_{Ds}})\tau_{mn}(\theta_{n_{Ds}})\sin(m\varphi_{n_{Ds}}) \end{matrix}}^{q_{mn}} \end{bmatrix} \tag{38}$$

$$\overline{\overline{\boldsymbol{C}}}^{\boldsymbol{scat}}_{\hat{\boldsymbol{r}}\hat{\boldsymbol{\varphi}}}(n_{Ds}) = \begin{bmatrix} \overbrace{0}^{p_{mn}} & \overbrace{if^3_{mn}(r_1)d^n_{0m}(\theta_1)\sin(m\varphi_1)}^{q_{mn}} \\ 0 & if^3_{mn}(r_2)d^n_{0m}(\theta_2)\sin(m\varphi_2) \\ \vdots & \vdots \\ 0 & if^3_{mn}(r_{n_{Ds}})d^n_{0m}(\theta_{n_{Ds}})\sin(m\varphi_{n_{Ds}}) \end{bmatrix} \quad (39)$$

At $\hat{\theta}$ incidence

$$\overline{\overline{\boldsymbol{C}}}^{\boldsymbol{scat}}_{\hat{\boldsymbol{\varphi}}\hat{\boldsymbol{\theta}}}(n_{Ds}) = \begin{bmatrix} \overbrace{f^{12}_{mn}(r_1)\tau_{mn}(\theta_1)\sin(m\varphi_1)}^{p_{mn}} & \overbrace{0 \quad f^{22}_{mn}(r_1)\pi_{mn}(\theta_1)\sin(m\varphi_1)}^{q_{mn}} \\ f^{12}_{mn}(r_2)\tau_{mn}(\theta_2)\sin(m\varphi_2) & 0 \quad f^{22}_{mn}(r_2)\pi_{mn}(\theta_2)\sin(m\varphi_2) \\ \vdots & \vdots \\ f^{12}_{mn}(r_{n_{Ds}})\tau_{mn}(\theta_{n_{Ds}})\sin(m\varphi_{n_{Ds}}) & 0 \quad f^{22}_{mn}(r_{n_{Ds}})\pi_{mn}(\theta_{n_{Ds}})\sin(m\varphi_{n_{Ds}}) \end{bmatrix} \quad (40)$$

$$\overline{\overline{\boldsymbol{C}}}^{\boldsymbol{scat}}_{\hat{\boldsymbol{\theta}}\hat{\boldsymbol{\theta}}}(n_{Ds}) = \begin{bmatrix} \overbrace{-f^{12}_{mn}(r_1)\pi_{mn}(\theta_1)\cos(m\varphi_1)}^{p_{mn}} & \overbrace{-\frac{1}{2}f^{22}_{0n}(r_1)\tau_{mn}(\theta_1) \quad -f^{22}_{mn}(r_1)\tau_{mn}(\theta_1)\cos(m\varphi_1)}^{q_{mn}} \\ -f^{12}_{mn}(r_2)\pi_{mn}(\theta_2)\cos(m\varphi_2) & -\frac{1}{2}f^{22}_{0n}(r_2)\tau_{mn}(\theta_2) \quad -f^{22}_{mn}(r_2)\tau_{mn}(\theta_2)\cos(m\varphi_2) \\ \vdots & \vdots \\ -f^{12}_{mn}(r_{n_{Ds}})\pi_{mn}(\theta_{n_{Ds}})\cos(m\varphi_{n_{Ds}}) & -\frac{1}{2}f^{22}_{0n}(r_{n_{Ds}})\tau_{mn}(\theta_{n_{Ds}}) \quad -f^{22}_{mn}(r_{n_{Ds}})\tau_{mn}(\theta_{n_{Ds}})\cos(m\varphi_{n_{Ds}}) \end{bmatrix} \quad (41)$$

$$\overline{\overline{\boldsymbol{C}}}^{\boldsymbol{scat}}_{\hat{\boldsymbol{r}}\hat{\boldsymbol{\theta}}}(n_{Ds}) = \begin{bmatrix} \overbrace{0}^{p_{mn}} & \overbrace{\frac{1}{2}f^3_{0n}(r_1)d^n_{00}(\theta_1) \quad f^3_{mn}(r_1)d^n_{0m}(\theta_1)\cos(m\varphi_1)}^{q_{mn}} \\ 0 & \frac{1}{2}f^3_{0n}(r_2)d^n_{00}(\theta_2) \quad f^3_{mn}(r_2)d^n_{0m}(\theta_2)\cos(m\varphi_2) \\ \vdots & \vdots \\ 0 & \frac{1}{2}f^3_{0n}(r_{n_{Ds}})d^n_{00}(\theta_{n_{Ds}}) \quad f^3_{mn}(r_{n_{Ds}})d^n_{0m}(\theta_{n_{Ds}})\cos(m\varphi_{n_{Ds}}) \end{bmatrix} \quad (42)$$

where

$$f^{11}_{mn}(r) = 2(-1)^{m+1}d_n h^{(1)}_n(kr) \quad (43)$$

$$f^{21}_{mn}(r) = 2(-1)^m id_n \frac{d\left[krh^{(1)}_n(kr)\right]}{krd[kr]} \quad (44)$$

$$f^3_{mn}(r) = 2(-1)^m d_{n'} \frac{h^{(1)}_n(kr)}{kr} \quad (45)$$

where $1 \le m \le n$ throughout equations (37)–(42).

2.2.1.3. The Left Generalized Inversion of $\overline{\overline{\boldsymbol{C}}}^{\boldsymbol{scat}}_{\hat{\boldsymbol{p}}}$

[15] The kernel of computing the scattered coefficient vector is to invert equations (29) and (35), which is defined as

$$\left[\overline{\overline{\boldsymbol{C}}}^{scat}_{\hat{p}}(n_{Ds})\right]^{-1}\overline{\overline{\boldsymbol{C}}}^{\boldsymbol{scat}}_{\hat{p}}(n_{Ds}) = \boldsymbol{I}_{\boldsymbol{n_{Ds}}} \quad (46)$$

Therefore

$$\begin{bmatrix} \boldsymbol{p_{mn}}(\theta_i,\hat{p}) \\ \boldsymbol{q}_{mn}(\theta_i,\hat{p}) \end{bmatrix} = \left[\overline{\overline{\boldsymbol{C}}}^{\boldsymbol{scat}}_{\hat{p}}(n_{Ds})\right]^{-1}\begin{bmatrix} \boldsymbol{S}_{\hat{\boldsymbol{\varphi}}\hat{\boldsymbol{p}}}(\boldsymbol{\theta_s},\theta_i) \\ \boldsymbol{S}_{\hat{\boldsymbol{\theta}}\hat{\boldsymbol{p}}}(\boldsymbol{\theta_s},\theta_i) \end{bmatrix} \quad (47)$$

The inversion of the rectangular matrix can be stably computed using the Singular Value Decomposition (SVD) method. The number of the observation points has to be sufficient to make the linear equation-set over-determined.

In the near-zone, $\overline{\overline{\boldsymbol{C}}}^{\boldsymbol{scat}}_{\hat{p}}(n_{Ds})$ is a block upper triangular matrix since $\overline{\overline{\boldsymbol{C}}}^{\boldsymbol{scat}}_{\hat{\boldsymbol{r}}\hat{\boldsymbol{p}}}$ has zero columns versus $\boldsymbol{p_{mn}}$. Therefore, $\overline{\overline{\boldsymbol{C}}}^{\boldsymbol{scat}}_{\hat{\boldsymbol{r}}\hat{\boldsymbol{p}}}$ is inverted block-wisely to save the computation. We can write

$$\overline{\overline{\boldsymbol{C}}}^{\boldsymbol{scat}}_{\hat{p}}(n_{Ds}) = \begin{bmatrix} \overbrace{\boldsymbol{A}^{\boldsymbol{m_1}\times\boldsymbol{n_1}}_{11}}^{p_{mn}} & \overbrace{\boldsymbol{A}_{12}}^{q_{mn}} \\ 0 & \boldsymbol{A}^{\boldsymbol{m_2}\times\boldsymbol{n_2}}_{22} \end{bmatrix}, m_1 \ge n_1,\, m_2 \ge n_2 \quad (48)$$

where

$$\begin{bmatrix} \overline{\overline{\boldsymbol{A}}}_{11} & \overline{\overline{\boldsymbol{A}}}_{12} \end{bmatrix} = \begin{bmatrix} \overline{\overline{\boldsymbol{C}}}^{\boldsymbol{scat}}_{\hat{\varphi}\hat{p}} \\ \overline{\overline{\boldsymbol{C}}}^{\boldsymbol{scat}}_{\hat{\theta}\hat{p}} \end{bmatrix} \quad (49)$$

and

$$\begin{bmatrix} 0 & \overline{\overline{\boldsymbol{A}}}_{22} \end{bmatrix} = \overline{\overline{\boldsymbol{C}}}^{scat}_{\hat{r}\hat{p}} \quad (50)$$

Once the left generalized inversion of $\overline{\overline{A}}_{11}$ and $\overline{\overline{A}}_{22}$ (i.e., $\overline{\overline{A}}_{11}^{-}$ and $\overline{\overline{A}}_{22}^{-}$) are obtained, we can write $\left[\overline{\overline{C}}_{\hat{p}}^{scat}(n_{Ds})\right]^{-1}$ as

$$\left[\overline{\overline{C}}_{\hat{p}}^{scat}(n_{Ds})\right]^{-1} = \begin{bmatrix} \overline{\overline{A}}_{11}^{-} & -\overline{\overline{A}}_{11}^{-}\overline{\overline{A}}_{12}\overline{\overline{A}}_{22}^{-} \\ 0 & \overline{\overline{A}}_{22}^{-} \end{bmatrix} \tag{51}$$

Another important issue concerning the singularity of the coefficient matrix $\overline{\overline{C}}_{\hat{p}}^{scat}$ is worth noting in the near-zone case. $\overline{\overline{C}}_{\hat{p}}^{scat}$ is bounded and regular in the far-zone since it consists solely of Associated Legendre functions and their derivatives. However, it usually becomes numerically singular in the near-zone because the order of magnitude of Hankel functions and their derivatives vary significantly at different orders when the radius approaches the origin. In other words, columns of high orders can be significantly larger than those of low orders, which is equivalent to having many zero-columns. To circumvent this, we confine the observation points to a spherical surface that originates at the geometric center of the scatterer. Therefore, all the points have a unique radius parameter and $\overline{\overline{A}}_{ij}$ can be factorized into the product of a regular matrix and a diagonal matrix. For example

$$\overline{\overline{A}}_{22} = \begin{bmatrix} f_{01}^{3'}(r)d_{00}^{n}(\theta_1) & \cdots & f_{mn}^{3'}(r_1)d_{0m}^{n}(\theta_1)\cos(m\varphi_1) \\ f_{01}^{3'}(r)d_{00}^{n}(\theta_2) & \cdots & f_{mn}^{3'}(r_2)d_{0m}^{n}(\theta_2)\cos(m\varphi_2) \\ \vdots & \ddots & \vdots \\ f_{01}^{3'}(r)d_{00}^{n}(\theta_{n_{Ds}}) & \cdots & f_{mn}^{3'}(r_{n_{Ds}})d_{0m}^{n}(\theta_{n_{Ds}})\cos(m\varphi_{n_{Ds}}) \end{bmatrix} \cdot \boldsymbol{Diag}\begin{bmatrix} \frac{h_1^{(1)}(kr)}{kr} & \cdots & \frac{h_n^{(1)}(kr)}{kr} \end{bmatrix} = \overline{\overline{\boldsymbol{P}}}_{22}(\overline{\boldsymbol{\theta}}, \overline{\boldsymbol{\varphi}})\overline{\overline{D}}_{22}(r) \tag{52}$$

where, $f_{mn}^{3'}$ is $f_{mn}^{3}(r)$ without the radius parameterized Hankel function factor $\frac{h_n^{(1)}(kr)}{kr}$ Similarly, we have

$$\overline{\overline{A}}_{11} = \overline{\overline{\boldsymbol{P}}}_{11}(\overline{\boldsymbol{\theta}}, \overline{\boldsymbol{\varphi}})\overline{\overline{\boldsymbol{D}}}_{11}(r) \tag{53}$$

and

$$\overline{\overline{A}}_{12} = \overline{\overline{\boldsymbol{P}}}_{12}(\overline{\theta}, \overline{\varphi}, r)\overline{\overline{\boldsymbol{D}}}_{12}(r) \tag{54}$$

$\overline{\overline{\boldsymbol{P}}}_{12}(\overline{\theta}, \overline{\varphi}, r)$ has an r factor of $\frac{d[krh_n^{(1)}(kr)]}{d[kr]}/h_n^{(1)}(kr)$ but is also regular. Then we replace $\overline{\overline{A}}_{ij}$ in equation (51) by $\overline{\overline{\boldsymbol{P}}}_{ij}$ to solve for $\begin{bmatrix} \boldsymbol{p_{mn}} \\ \boldsymbol{q_{mn}} \end{bmatrix}$, multiplying both sides of equation (35) by $\overline{\overline{\boldsymbol{P}}}^{-}$ and normalizing the result by the corresponding elements of the diagonal matrix in equation (52). The purpose of the normalization is to avoid any matrix multiplication by the Hankel functions, which amplifies the round error of the numerical matrix inversion in equation (51).

[16] The scattering amplitudes, $\boldsymbol{S}_{\hat{\varphi}\hat{p}}(\boldsymbol{\theta_s}, \theta_i)$ and $\boldsymbol{S}_{\hat{\theta}\hat{p}}(\boldsymbol{\theta_s}, \theta_i)$, on the left hand side of equations (29) and (35) are obtained using the existing EM model to be discussed in section 3.2. Inverting $\overline{\overline{C}}_{\hat{p}}^{scat}$ is the most time-consuming and memory-occupying step in the whole procedure of the matrix inversion approach since the size of the matrix is $O(n_{\max}^2)$. Fortunately, this step needs performing only twice at a given $n_{\max}$ because one scattered set of angles and polarizations is sufficient to calculate $\begin{bmatrix} \boldsymbol{p_{mn}} \\ \boldsymbol{q_{mn}} \end{bmatrix}$ at any incidence.

2.2.2. Computing the T-Matrix Elements Using the Scattered Coefficient Vectors

2.2.2.1. The T-Matrix of Arbitrary Axial Symmetric Shapes

[17] Considering the block-diagonal property, T-matrix elements can be calculated block-by-block with respect to the m-index by inverting equation (5). As mentioned in 2.2.1, $\begin{bmatrix} \boldsymbol{p_{mn}} \\ \boldsymbol{q_{mn}} \end{bmatrix}$ depends solely on the incident wave and particle, therefore, it is a function of the direction and polarization of the incidence. The block gets its maximum size of $2n_{\max} \times 2n_{\max}$ when $m = 0$ or 1. Therefore, the number of the directions of incidence should be $n_{\max}$ since we employ both polarizations. Since the azimuth angle of the incident wave is set to zero, we can write the coefficient matrix of the m-order incident wave as

$$\overline{\overline{\boldsymbol{C}}}_{\boldsymbol{m}}^{\boldsymbol{inc}} = \begin{bmatrix} a_{mn}(\theta_1^i, \hat{\varphi}) & a_{mn}(\theta_2^i, \hat{\varphi}) & \cdots & a_{mn}(\theta_{n_{max}}^i, \hat{\varphi}) & a_{mn}(\theta_1^i, \hat{\theta}) & \cdots & a_{mn}(\theta_{n_{max}}^i, \hat{\theta}) \\ b_{mn}(\theta_1^i, \hat{\varphi}) & b_{mn}(\theta_2^i, \hat{\varphi}) & \cdots & b_{mn}(\theta_{n_{max}}^i, \hat{\varphi}) & b_{mn}(\theta_1^i, \hat{\theta}) & \cdots & b_{mn}(\theta_{n_{max}}^i, \hat{\theta}) \end{bmatrix} \tag{55}$$

and the corresponding matrix on the left hand side of the equation as

$$\overline{\overline{\boldsymbol{PQ}}}_{\boldsymbol{m}}^{\boldsymbol{inc}} = \begin{bmatrix} p_{mn}(\theta_1^i, \hat{\varphi}) & p_{mn}(\theta_2^i, \hat{\varphi}) & \cdots & p_{mn}(\theta_{n_{max}}^i, \hat{\varphi}) & p_{mn}(\theta_1^i, \hat{\theta}) & \cdots & p_{mn}(\theta_{n_{max}}^i, \hat{\theta}) \\ q_{mn}(\theta_1^i, \hat{\varphi}) & q_{mn}(\theta_2^i, \hat{\varphi}) & \cdots & q_{mn}(\theta_{n_{max}}^i, \hat{\varphi}) & q_{mn}(\theta_1^i, \hat{\theta}) & \cdots & q_{mn}(\theta_{n_{max}}^i, \hat{\theta}) \end{bmatrix} \tag{56}$$

Equation (5) is rewritten in its "block-split" form

$$\overline{\overline{\boldsymbol{PQ}}}_{\boldsymbol{m}}^{inc} = \overline{\overline{\boldsymbol{T}}}_{\boldsymbol{m}}\overline{\overline{\boldsymbol{C}}}_{\boldsymbol{m}}^{\boldsymbol{inc}} \tag{57}$$

Note that $\overline{\overline{\boldsymbol{C}}}_{\boldsymbol{m}}^{\boldsymbol{inc}}$ is nonsquare unless $m = 0$ or 1. Therefore, we need to use the SVD decomposition again to get the right

generalized inversion of $\overline{\overline{\boldsymbol{C}}}_{\boldsymbol{m}}^{\boldsymbol{inc}}$ when $m > 1$. We denote $\left(\overline{\overline{\boldsymbol{C}}}_{\boldsymbol{m}}^{\boldsymbol{inc}}\right)^{-1}$ as the right generalized inversion of $\overline{\overline{\boldsymbol{C}}}_{\boldsymbol{m}}^{\boldsymbol{inc}}$, which obeys

$$\overline{\overline{\boldsymbol{C}}}_{m}^{inc}\left(\overline{\overline{\boldsymbol{C}}}_{m}^{inc}\right)^{-1} = \boldsymbol{I}_{n_{max}-m+1} \tag{58}$$

Substituting equation (58) into (57), we obtain the T-matrix elements

$$\overline{\overline{\boldsymbol{T}}}_{m} = \begin{bmatrix} \boldsymbol{p_{mn}} \\ \boldsymbol{q_{mn}} \end{bmatrix}\left(\overline{\overline{\boldsymbol{C}}}_{\boldsymbol{m}}^{\boldsymbol{inc}}\right)^{-1} \tag{59}$$

2.2.2.2. The T-Matrix of Axial Symmetric Shape With an Orthogonal Symmetric Plane

[18] Many particles of interest in remote sensing are not only axial symmetric but also plane symmetric with respect to the x-o-y plane. The plane symmetry produces many zeros in the T-matrix, i.e.,

$$T_{mnn'}^{ij} = \begin{cases} 0, & otherwise \\ otherwise, & i+j \equiv n+n' \bmod(2) \end{cases}, i,j = 1,2 \tag{60}$$

Equation (5) can be split into two equations using equation (60), i.e.,

$$\begin{bmatrix} p_{mm} \\ p_{m(m+2)} \\ \vdots \\ q_{m(m+1)} \\ q_{m(m+3)} \\ \vdots \end{bmatrix} = \begin{bmatrix} T_{mmm}^{11} & T_{mm(m+2)}^{11} & \cdots & T_{mm(m+1)}^{12} & T_{mm(m+3)}^{12} & \cdots \\ T_{m(m+2)m}^{11} & T_{m(m+2)(m+2)}^{11} & \cdots & T_{m(m+2)(m+1)}^{12} & T_{m(m+2)(m+3)}^{12} & \cdots \\ \vdots & \vdots & \ddots & \vdots & \vdots & \ddots \\ T_{m(m+1)m}^{21} & T_{m(m+1)(m+2)}^{21} & \cdots & T_{m(m+1)(m+1)}^{22} & T_{m(m+1)(m+3)}^{22} & \cdots \\ T_{m(m+3)m}^{21} & T_{m(m+3)(m+2)}^{21} & \cdots & T_{m(m+3)(m+1)}^{22} & T_{m(m+3)(m+3)}^{22} & \cdots \\ \vdots & \vdots & \ddots & \vdots & \vdots & \ddots \end{bmatrix} \begin{bmatrix} a_{mm} \\ a_{m(m+2)} \\ \vdots \\ b_{m(m+1)} \\ b_{m(m+3)} \\ \vdots \end{bmatrix} \tag{61}$$

and

$$\begin{bmatrix} p_{m(m+1)} \\ p_{m(m+3)} \\ \vdots \\ q_{mm} \\ q_{m(m+2)} \\ \vdots \end{bmatrix} = \begin{bmatrix} T_{m(m+1)(m+1)}^{11} & T_{m(m+1)(m+3)}^{11} & \cdots & T_{m(m+1)m}^{12} & T_{m(m+1)(m+2)}^{12} & \cdots \\ T_{m(m+3)(m+1)}^{11} & T_{m(m+3)(m+3)}^{11} & \cdots & T_{m(m+3)m}^{12} & T_{m(m+3)(m+2)}^{12} & \cdots \\ \vdots & \vdots & \ddots & \vdots & \vdots & \ddots \\ T_{mm(m+1)}^{21} & T_{mm(m+3)}^{21} & \cdots & T_{mmm}^{22} & T_{mm(m+2)}^{22} & \cdots \\ T_{m(m+2)(m+1)}^{21} & T_{m(m+2)(m+3)}^{21} & \cdots & T_{m(m+2)m}^{22} & T_{m(m+2)(m+2)}^{22} & \cdots \\ \vdots & \vdots & \ddots & \vdots & \vdots & \ddots \end{bmatrix} \begin{bmatrix} a_{m(m+1)} \\ a_{m(m+3)} \\ \vdots \\ b_{mm} \\ b_{m(m+2)} \\ \vdots \end{bmatrix} \tag{62}$$

In this circumstance, we compute $\frac{n_{max}}{2}$ instead of $n_{\max}$ directions of incidence, which saves half of the simulation time cost by the EM model.

3. Results and Discussion

3.1. Numerical Issues

[19] By optimally choosing a distribution of discrete incidence, scattering angles and polarizations we can circumvent $\overline{\overline{\boldsymbol{C}}}_{\hat{p}}^{scat}$ and $\overline{\overline{\boldsymbol{C}}}_{m}^{inc}$ from being singular. In practice, we found that when

$$n_{Ds} = n_{max}(n_{max}+2) \tag{63}$$

which equals the number of unknowns, and when the scattered directions are evenly randomly distributed in the sphere, i.e., 4π solid angle, the matrix is always regular. In the far-zone case, the size of the matrix for SVD is about $2n_{Ds} \times n_{Ds}$ considering both scattered polarizations. While in the near-zone case, they are $n_{Ds} \times \frac{n_{Ds}}{2}$ and $2n_{Ds} \times \frac{n_{Ds}}{2}$. Although regular grids that consist of evenly spaced latitudes and longitudes of the scattering angles are simple, they make $\overline{\overline{\boldsymbol{C}}}_{p'}^{scat}$ singular. In this case, the ratio of the maximum and minimum eigen values is over 10^{21} while our evenly randomly distributed strategy yields the ratio always less than 10^5. Both $\hat{\varphi}$ and $\hat{\theta}$ polarized incident waves have to be employed in equations (57) because either polarization has a zero column when $m = 0$. The least sufficient incidences to make all $\overline{\overline{\boldsymbol{C}}}_{m}^{inc}$ matrices regular are $n_{\max}$ evenly spaced zeniths from $0 - \pi$ in the rotational only symmetrical case and $n_{\max}/2$ evenly spaced zeniths from $0 - \pi/2$ in the rotational plus plane symmetric case. Since with axially symmetrical shapes, the scattering property with respect to the azimuth angle depends solely on the relative azimuth angle (the azimuth angle difference between the scattering and the incidence), we can set all the angles of incidence to zero azimuth. The scattering dependence of the azimuth angle is accounted for by the distribution of the scattered azimuth angles. On the other hand, if the particle of interest is not axially symmetrical, multiple incidence azimuth angles have to be employed in this matrix inversion approach.

[20] The truncation order, $n_{\max}$, significantly affects the computing accuracy. Previous studies [*Loke et al.*, 2009;

Table 1. EM Model n_{max}

	n_{max} for Near Field	n_{max} for Far Field	EM Model
Figures 2a and 2b	23	15	MOM
Figures 2c and 2d	35	30	PO
Figures 3a and 3b	25	8	MOM
Figures 3c and 3d	35	30	MOM
Figures 3e and 3f	40	35	MLFMM

Nieminen et al., 2003] suggest that n_{max} should be proportional to the largest dimension of the particle, say

$$n_{max} = kr_0 \tag{64}$$

or

$$n_{max} = kr_0 + 3\sqrt[3]{kr_0} \tag{65}$$

where r_0 is the length of the largest dimension of the particle.

[21] In the calculation, we find the same trend of n_{max} toward kr_0. However, the convergence seems to require an even larger n_{max} because of the too extremely shaped particle. Therefore, we have added 20 to the right hand side of (65) and obtained excellent results if the T-matrix is solved for in the far-zone. If the region of matching is close to the minimum sphere, the n_{max} must be increased by a few increments because the effect of the high order terms becomes larger. Table 1 lists the necessary n_{max} for the objects in Figures 2 and 3.

[22] Tested on a 4GB RAM Lenovo mt8000, the memory cost is affordable for the SVD step when $n_{max} \leq 50$. Meanwhile, it is not difficult to tell whether n_{max} is sufficient by comparing the scattering coefficients calculated by the mentioned EM model and those by the proposed T-matrix framework. It is obvious that the proposed T-matrix framework and the employed EM model yield essentially identical results.

[23] Despite the completely different computational steps required between the direct T-matrix and the matrix inversion approach, difficulties occur at large n_{max}. As mentioned in section 1, the direct calculation of the T-matrix of particles with large aspect ratios could not proceed in the numerical integration step because the Bessel functions of the complex variable will oscillate drastically and the Hankel functions increase sharply when the radius approaches the origin. Moreover, the integrated value of large n_{max} is many orders of magnitude larger than that of small n_{max} in the $Rg\overline{\overline{Q}}$ and $\overline{\overline{Q}}$ matrices, which makes the inversion of the $\overline{\overline{Q}}$ matrix ill-conditioned and thus inaccurate [*Mishchenko et al.*, 1996]. Attempts to resolve these problems by calculating T-matrix directly are practically intractable. With the matrix inversion approach, difficulty with large n_{max} comes mainly from the SVD step, which is typically limited by the finite memory.

3.2. The Existing EM Model

[24] The existing EM model used to calculate scattering amplitudes is arbitrary in principle but must be adequately precise to solve for the extreme shapes of various dimensions. Among a variety of algorithms and methods, we have chosen a commercially available software, FEKO, (Feldberechnung bei Korpern mit beliebiger Oberflache) that integrates the MOM Multilevel Fast Multipole Method (MLFMM) and PO. For dielectrically small objects, one can use the default MOM solution to obtain the best accuracy. If the object is relatively large, one can choose MLFMM alternatively for the efficiency purpose. In case the frequency is too high or the object is too large, the PO is the ultimate option. In this study, we use the MOM and PO to calculate the scattering of a circular disk at L-band and Ku-band respectively. For prolate cylinders at L-band, we use the MOM for aspect ratios between 1 and10, and the MLFMM for aspect ratios ranging from 20 to50.

3.3. Result

[25] Once the T-matrix of a given object is obtained, the scattering coefficients of an arbitrary orientation with the directions of any incidence and scattering can be easily computed by rotating the coordinate system [*Mishchenko*, 1991]. Therefore, it is convenient to compare the scattering coefficients calculated from the existing EM model and those from the proposed T-matrix framework. In this section, the scattering coefficients of several cylinders of extreme aspect ratios and large dielectric dimensions are tested. The chosen aspect ratios range from 0.02 to 200 to cover the typical size of leaves and branches. The dielectric constant is set to 28+14i which is empirically [*Ulaby et al.*, 1987] converted from 0.85 gravimetric water content of vegetation.

[26] Figure 1 describes the directions of the scattering and incidence, which are used for validation throughout Figures 2 and 3. The bistatic curve is excited at $\theta^i = 30°$ and $\varphi^i = 0°$; the RCS curve is compared at the backward directions $\theta^s = 0 \sim 90°$ and $\varphi^s = 180 + 40°$. In Figure 2, the T-matrix of a circular disk with 5-cm radius and 0.5-mm thickness is calculated at L and Ku bands, respectively. Then the T-matrix is used to calculate the scattering coefficients described in Figure 2. In Figure 3, we have validated the

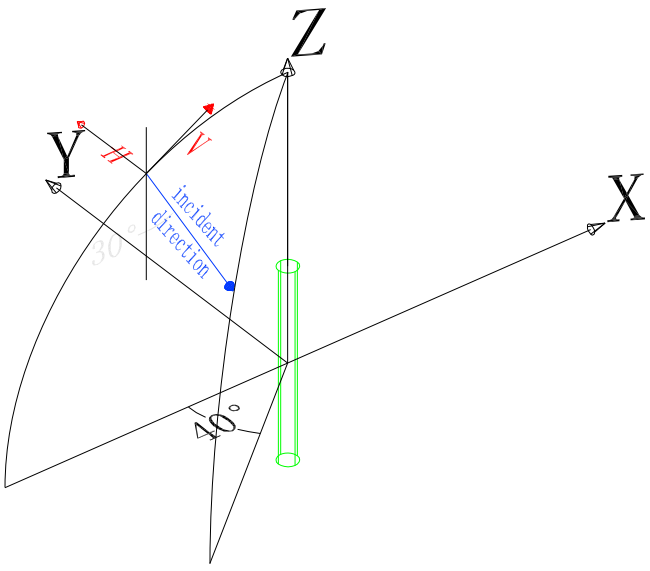

Figure 1. Directions of the scattering and incidence used in the validation through Figures 2 and 3. The object is centered at the origin. The excitation is within the x-o-z plane and the angle of incidence is 30°.

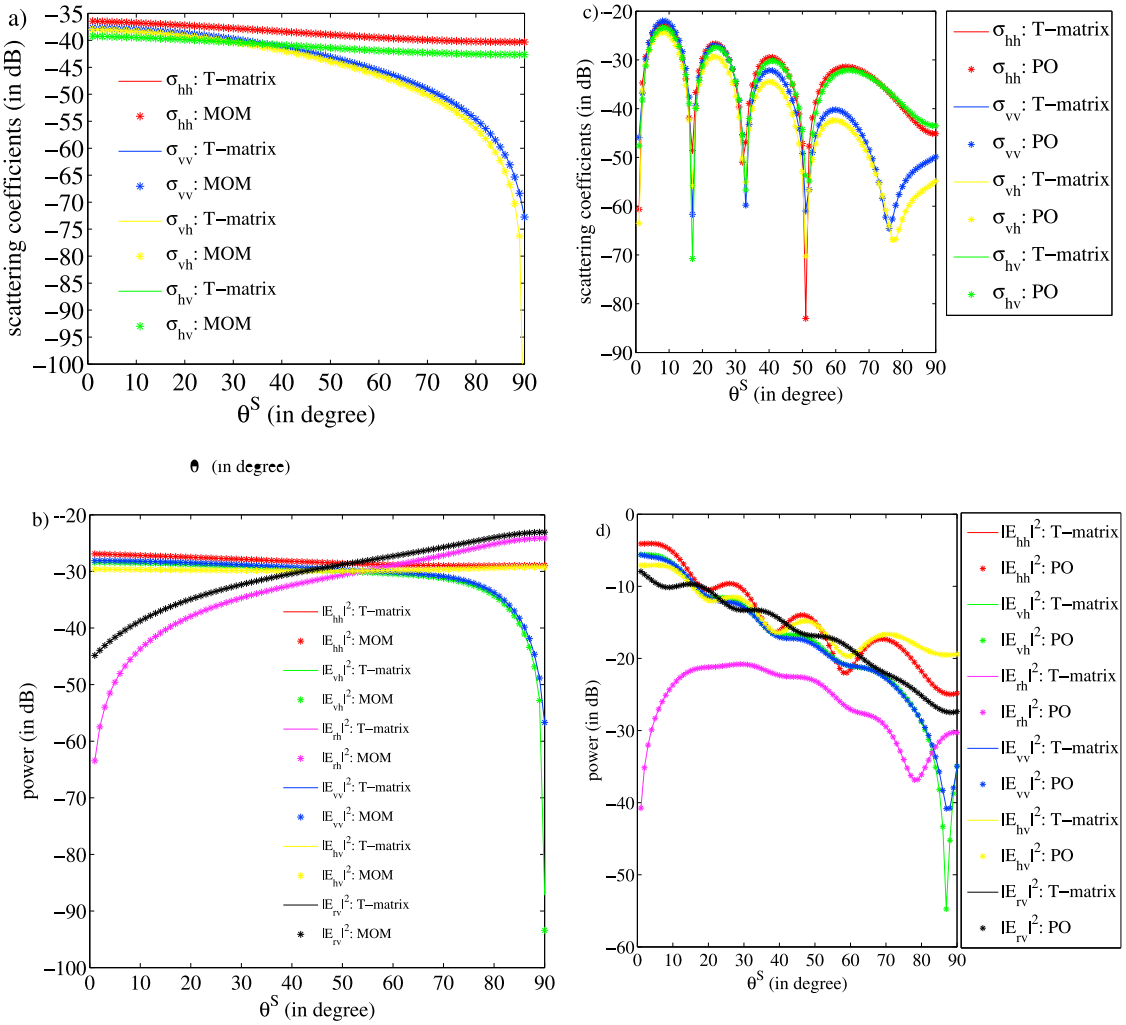

Figure 2. Scattering coefficients comparison of dielectric circular disk with an aspect ratio 200 at high frequency. The radius of the disk is 5 cm. (a) Far-zone field scattering coefficients at L-band; (b) r = 7 cm near-zone power at L-band; (c) far-zone field scattering coefficients at Ku-band; and (d) r = 7 cm near-zone power at Ku-band.

scattering of cylinders with 1-cm diameter and height at1, 20 and 50 cm respectively using the proposed approach. It should be noted that the PO approximation is used in Figures 2c and 2d in the EM model instead of the MOM due to the very high frequency, while the MOM is replaced by the MLFMM in Figures 3e and 3f to promote the efficiency. The validation is conducted both in the far-zone and in the near-zone.

[27] Results of the proposed method are identical to those of the existing EM model. Meanwhile, we found that the T-matrix solved at the near-zone can correctly output the scattering coefficients in the far-zone, whereas, the T-matrix computed using the far-zone coefficients is only valid in the far-zone. Moreover, the T-matrix solved at a certain distance can give correct results in an equal or further region only and produce unacceptable error in the nearer region. Therefore, we have excluded the far field comparisons that use the T-matrix solved in the far-zone because they are identical to the corresponding ones that use the T-matrix solved in the near-zone. Consequently, the near-zone match is recommended in most cases. The far-zone match applies only if the far-zone scattering is required.

3.4. The Limitation of the Proposed Method

[28] The proposed method is somewhat limited by the conventional invalid region between the particle surface and the minimum circumscribing sphere not only because of the invalid expansion of the Green's function in this region, which can be circumvented by matching the boundary condition using the total field [*Doicu and Wriedt*, 2010; *Forestiere et al.*, 2011], but also due to the extreme shapes of the particles of interest. We have illustrated the electric field (E-field) distribution of the particle in Figure 3f on a 15 cm sphere in Figure 4. It is observed that the E-field increases sharply when the observation points approach the polar of the sphere because the points around the polar are closer to the surface of the particle. This implies that the E-field distribution on a spherical surface is strongly affected by the shape of the particle, which numerically results in the inaccuracy of computing the very near field of an extremely

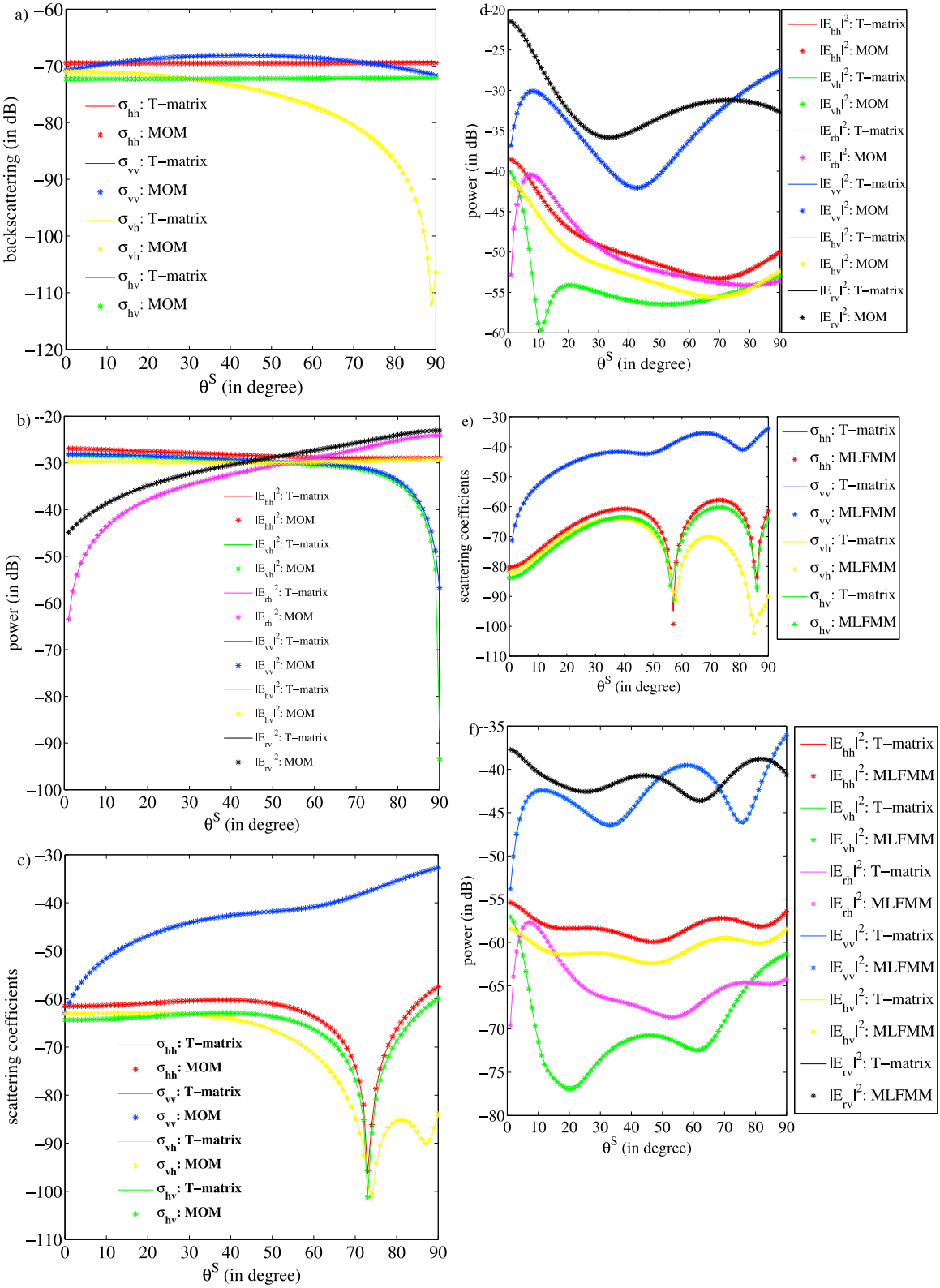

Figure 3. Scattering coefficients comparison of dielectric cylinders of 1 cm diameter at L-band. (a) Far-zone field comparison with the aspect ratio being 1; (b) 9 mm near-zone field comparison of the same cylinder of Figure 3a; (c) far-zone field comparison with the aspect ratio being 1/20; (d) 12 cm near-zone field comparison with the parameters being the same as in Figure 3c; (e) the far-zone comparison with the aspect ratio being 1/50; (f) 30 cm near-zone comparison the parameters being the same as in Figure 3e.

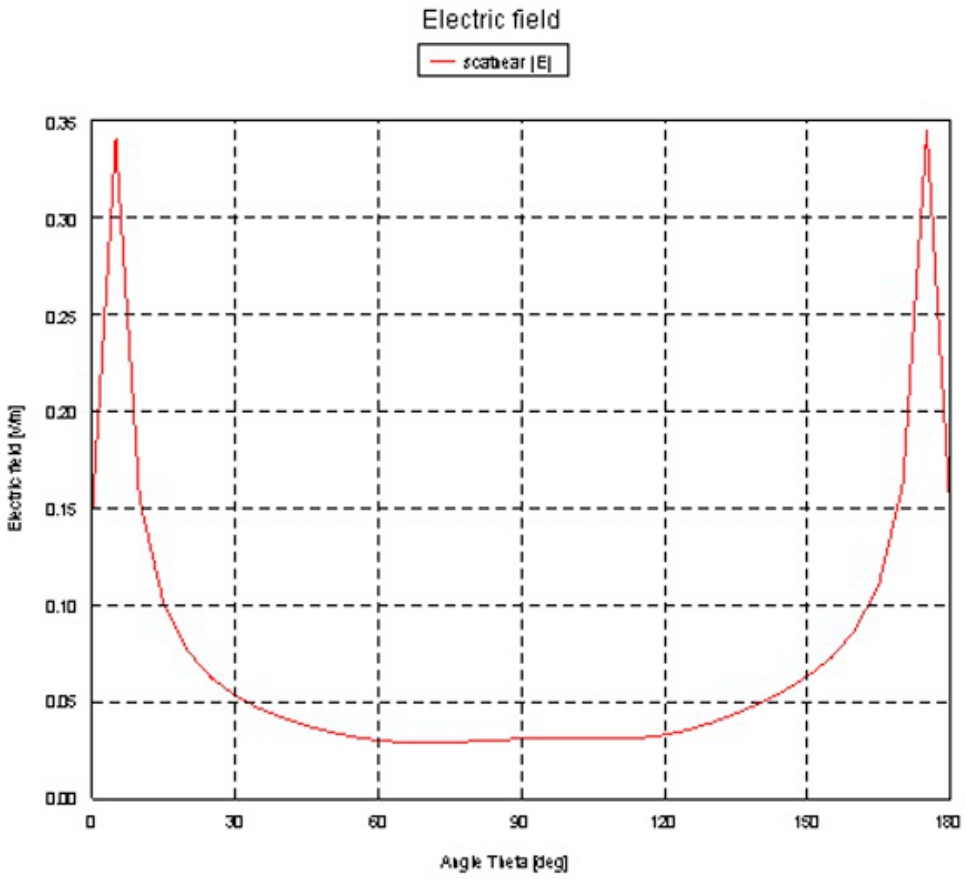

Figure 4. Electric field distribution of the prolate cylinder described in Figure 3f on a sphere with a radius of 15 cm. The azimuth angle is 0. For other azimuth angle, the trend of the curve is similar.

shaped particle using the LS T-matrix. The radius parameter is constant if the observation points are on a single sphere since the LS T-matrix has only one origin located at the geometric center of the particle. The Associated Legendre functions and their derivatives have to account for such a sharp increase of the E-field, which requires almost infinite orders because the Associated Legendre functions and their derivatives are regular and bounded. On the other hand, if the discrete sources (DS) T-matrix [*Doicu et al.*, 2000] is employed, the Hankel functions and their derivatives can produce this sharp increase because different orders of them have different origins and they essentially increase sharply toward their origin.

4. Summary

[29] In conclusion, the proposed T-matrix calculation method devises a simple yet powerful solution to the scattering problem of extreme-shaped and dielectrically large particles in the framework of the T-matrix. Results of the proposed T-matrix framework are verified to be identical to those of the existing EM model. Therefore, the accuracy of the proposed method relies essentially on the employed EM model. The scattering property of the extremely shaped particles is accurately presented in the resonant and PO regions by the T-matrix calculated using the proposed matrix inversion approach when the direct T-matrix calculation is too difficult to converge. Furthermore, the proposed framework enables fast computation of the scattering of arbitrarily oriented particles illuminated by radar from any direction. Most importantly, it potentially improves the accuracy of assessing the total scattering of the crown layer by including the interactions of the canopy materials. The solving technique is not unique since the scattered coefficients can be solved in either the far-zone or the near-zone. Moreover, we conclude that the T-matrix solved in the near-zone can output correct scattering fields anywhere further than the solving spherical surface while the T-matrix solved in the far-zone is not trustworthy in the nearer region. The far-zone solving technique should be employed only when the far-zone scattering is needed to save computation. Future research may extend to applying the matrix inversion approach to the DS T-matrix framework in order to include the region between the particle surface and the minimum circumscribing sphere and to better evaluate the multiple scattering in the vegetation layer. In addition, as pointed out by *Nieminen et al.* [2003], though FDTD is considered less efficient than many other EM methods, such as Discrete Dipole (DDA) [*Mackowski*, 2002] and MOM, it requires meshing not only the region inside the dielectric medium but also the surrounding free space when solving the scattering problem in an open region, it can calculate the scattering within a bandwidth instead of at a single frequency. Variable frequencies at a fixed size are electromagnetically equivalent to a fixed frequency with variable sizes. However, in vegetation remote sensing, this strategy is useful

when the lengths at all dimensions change at the same rate for a given type of particle.

Appendix A: Definitions of The Spherical Harmonics

[30] The complete formulas of the spherical harmonics can be found in the book [*Mishchenko et al.*, 2005] and are listed here for reference.

$$a_{mn} = 4\pi(-1)^m i^n d_n \vec{E}_0 \cdot \vec{C}^*_{mn}(\theta') e^{-im\varphi'} \tag{A1}$$

$$b_{mn} = 4\pi(-1)^m i^{n-1} d_n \vec{E}_0 \cdot \vec{B}^*_{mn}(\theta') e^{-im\varphi'} \tag{A2}$$

$$Rg\vec{M}_{mn}(kr,\theta,\varphi) = (-1)^m d_n j_n(kr) \vec{C}_{mn}(\theta) e^{im\varphi} \tag{A3}$$

$$Rg\vec{N}_{mn}(kr,\theta,\varphi) = (-1)^m \left\{ d'_n \frac{j_n(kr)}{kr} \vec{P}_{mn}(\theta) + d_n \frac{1}{kr} \frac{d[krj_n(kr)]}{d(kr)} \vec{B}_{mn}(\theta) \right\} e^{im\varphi} \tag{A4}$$

where j_n is the first kind of spherical Bessel function and

$$d_n = \sqrt{\frac{2n+1}{4\pi n(n+1)}} \tag{A5}$$

$$d'_n = \sqrt{\frac{(2n+1)n(n+1)}{4\pi}} \tag{A6}$$

$$\vec{B}_{mn}(\theta) = \hat{\theta}\tau_{mn}(\theta) + \hat{\varphi} i \pi_{mn}(\theta) \tag{A7}$$

$$\vec{C}_{mn}(\theta) = \hat{\theta} i \pi_{mn}(\theta) - \hat{\varphi}\tau_{mn}(\theta) \tag{A8}$$

$$\vec{P}_{mn}(\theta) = \hat{r} d^n_{0m}(\theta) \tag{A9}$$

$$\pi_{mn}(\theta) = \frac{m}{\sin\theta} d^n_{0m}(\theta) \tag{A10}$$

$$\tau_{mn}(\theta) = \frac{d}{d\theta} d^n_{0m}(\theta) \tag{A11}$$

where $d^n_{0m}(\theta)$ is the Wigner d-function which has the following relationship to the Associated Legendre function, which in practical calculation, avoids the overflow of the Associated Legendre function

$$d^n_{0m}(\theta) = (-1)^m \sqrt{\frac{(n-m)!}{(n-m)!}} P^m_n(\cos\theta) \tag{A12}$$

From (5.37) by *Mishchenko et al.* [2005], we obtain

$$\overline{\overline{\boldsymbol{T}}}_{-m} = \begin{bmatrix} \overline{\overline{\boldsymbol{T}}}^{11}_{mnn'} & -\overline{\overline{\boldsymbol{T}}}^{12}_{mnn'} \\ -\overline{\overline{\boldsymbol{T}}}^{21}_{mnn'} & \overline{\overline{\boldsymbol{T}}}^{22}_{mm'n'} \end{bmatrix} \tag{A13}$$

Using negative m in equation (A11), we have

$$\begin{bmatrix} \boldsymbol{p}_{-mn} \\ \boldsymbol{q}_{-mn} \end{bmatrix} = \overline{\overline{\boldsymbol{T}}}_{-mnn'} \begin{bmatrix} \boldsymbol{a}_{-mn'} \\ \boldsymbol{b}_{-mn'} \end{bmatrix}, m \le n, n' \le n_{max} \tag{A14}$$

Letting the azimuth angle $\varphi' = 0$ in (equations A1) and (A2), and noting that [*Mishchenko et al.*, 2005]

$$\pi_{-mn} = (-1)^{m+1} \pi_{mn} \tag{A15}$$

$$\tau_{-mn} = (-1)^m \tau_{mn} \tag{A16}$$

we obtain

$$a_{mn} = 4\pi(-1)^{m+1} i^n d_n E^0_\varphi \tau_{mn}(\theta') \tag{A17}$$

$$b_{mn} = 4\pi(-1)^{m+1} i^n d_n E^0_\varphi \pi_{mn}(\theta') \tag{A18}$$

at $\hat{\varphi}$ polarized excitation. Substituting (equations A13) and (A14) into (A15) and (A16) with negative m index, we have

$$a_{-mn} = (-1)^m a_{mn} \tag{A19}$$

$$b_{-mn} = (-1)^{m+1} b_{mn} \tag{A20}$$

Substituting (equations A13), (A19) and (A20) into (A14), we obtain equations (14) and (15) in section 2.2.1. At $\hat{\theta}$ polarized incidence, equations (16) and (17) can be derived in the same way.

[31] **Acknowledgments.** This study was partially supported by the national science and technology support program (2012BAH29B03) and the national natural science foundation of (China2012BAC16B04, 41071221). The first author would like to express his gratitude to Michael I. Mishchenko for the kind help on the T-matrix theory and codes. Finally, the authors would like to express their condolences to the family of Peter C. Waterman (1928–2012), the creator of the T-matrix method.

References

Barber, P., and C. Yeh (1975), Scattering of electromagnetic waves by arbitrarily shaped dielectric bodies, *Appl. Opt.*, *14*(12), 2864–2872, doi:10.1364/AO.14.002864.

Bracaglia, M., P. Ferrazzoli, and L. Guerriero (1995), A fully polarimetric multiple scattering model for crops, *Remote Sens. Environ.*, *54*(3), 170–179, doi:10.1016/0034-4257(95)00151-4.

Chandrasekhar, S. (1950), *Radiative Transfer*, Clarendon, Oxford, U. K.

Doicu, A., and T. Wriedt (2010), Near-field computation using the null-field method, *J. Quant. Spectrosc. Radiat. Transf.*, *111*(3), 466–473, doi:10.1016/j.jqsrt.2009.10.003.

Doicu, A., Y. Eremin, and T. Wriedt (2000), *Acoustic and Electromagnetic Scattering Analysis Using Discrete Sources*, Academic, San Diego, Calif.

Eom, H., and A. Fung (1984), A scatter model for vegetation up to Ku-band, *Remote Sens. Environ.*, *15*(3), 185–200, doi:10.1016/0034-4257(84)90030-0.

Eom, H., and A. Fung (1986), Scattering from a random layer embedded with dielectric needles, *Remote Sens. Environ.*, *19*(2), 139–149, doi:10.1016/0034-4257(86)90067-2.

Foldy, L. L. (1945), The multiple scattering of waves. I. General theory of isotropic scattering by randomly distributed scatterers, *Phys. Rev.*, *67*(3–4), 107–119, doi:10.1103/PhysRev.67.107.

Forestiere, C., G. Iadarola, L. Dal Negro, and G. Miano (2011), Near-field calculation based on the T-matrix method with discrete sources, *J. Quant. Spectrosc. Radiat. Transf.*, *112*, 2384–2394, doi:10.1016/j.jqsrt.2011.05.009.

Fung, A. K. (1994), *Microwave Scattering and Emission Models and Their Applications*, Artech House, Boston.

Gürel, L., and W. C. Chew (1992), A recursive T-matrix algorithm for strips and patches, *Radio Sci.*, *27*(3), 387–401, doi:10.1029/91RS03054.

Harrington, R. (1987), The method of moments in electromagnetics, *J. Electromagn. Wave Appl.*, *1*(3), 181–200, doi:10.1163/156939387X00018.

Ishimaru, A. (1999), *Wave Propagation and Scattering in Random Media*, IEEE Press, New York.

Iskander, M. F., and A. Lakhtakia (1984), Extension of the iterative EBCM to calculate scattering by low-loss or lossless elongated dielectric objects, *Appl. Opt.*, *23*(6), 948–953, doi:10.1364/AO.23.000948.

Karam, M. A., A. K. Fung, and Y. M. M. Antar (1988), Electromagnetic wave scattering from some vegetation samples, *IEEE Trans. Geosci. Remote Sens.*, *26*(6), 799–808, doi:10.1109/36.7711.

Lakhtakia, A., M. F. Iskander, and C. H. Durney (1983), An iterative extended boundary-condition method for solving the absorption characteristics of lossy dielectric objects of large aspect ratios, *IEEE Trans. Microwave Theory Tech.*, *31*(8), 640–647, doi:10.1109/TMTT.1983.1131562.

Lakhtakia, A., V. K. Varadan, and V. V. Varadan (1984), Scattering by highly aspherical targets: EBCM coupled with reinforced orthogonalizations, *Appl. Opt.*, *23*(20), 3502–3504, doi:10.1364/AO.23.3502_1.

Lax, M. (1951), Multiple scattering of waves, *Rev. Mod. Phys.*, *23*(4), 287–310, doi:10.1103/RevModPhys.23.287.

Lee, J. S., and E. Pottier (2009), *Polarimetric Radar Imaging: From Basics to Applications*, CRC Press, Boca Raton, Fla., doi:10.1201/9781420054989.

LeVine, D., R. Meneghini, R. Lang, and S. Seker (1983), Scattering from arbitrarily oriented dielectric disks in the physical optics regime, *J. Opt. Soc. Am.*, *73*(10), 1255–1262, doi:10.1364/JOSA.73.001255.

Loke, V. L. Y., T. A. Nieminen, N. R. Heckenberg, and H. Rubinsztein-Dunlop (2009), T-matrix calculation via discrete dipole approximation, point matching and exploiting symmetry, *J. Quant. Spectrosc. Radiat. Transf.*, *110*(14–16), 1460–1471, doi:10.1016/j.jqsrt.2009.01.013.

Lu, C. C., W. C. Chew, Y. Wang, and L. Tsang (1993), The application of recursive aggregate T-matrix algorithm in the Monte Carlo simulations of the extinction rate of random distribution of particles, in *Antennas and Propagation Society International Symposium, 1993. AP-S. Digest*, pp. 1292–1294, IEEE, Ann Arbor, Mich.

Mackowski, D. W. (1994), Calculation of total cross-sections of multiple-sphere clusters, *J. Opt. Soc. Am. A Opt. Image Sci. Vis.*, *11*(11), 2851–2861, doi:10.1364/JOSAA.11.002851.

Mackowski, D. W. (2002), Discrete dipole moment method for calculation of the T-matrix for nonspherical particles, *J. Opt. Soc. Am. A Opt. Image Sci. Vis.*, *19*(5), 881–893, doi:10.1364/JOSAA.19.000881.

Michaeli, A. (1984), Equivalent edge currents for arbitrary aspects of observation, *IEEE Trans. Antennas Propag.*, *32*(3), 252–258, doi:10.1109/TAP.1984.1143303.

Mishchenko, M. I. (1990), Extinction of light by randomly oriented nonspherical grains, *Astrophys. Space Sci.*, *164*(1), 1–13, doi:10.1007/BF00653546.

Mishchenko, M. I. (1991), Light-scattering by randomly oriented axially symmetrical particles, *J. Opt. Soc. Am. A Opt. Image Sci. Vis.*, *8*(6), 871–882, doi:10.1364/JOSAA.8.000871.

Mishchenko, M. I. (1993), Light-scattering by size shape distributions of randomly oriented axially symmetrical particles of a size comparable to a wavelength, *Appl. Opt.*, *32*(24), 4652–4666, doi:10.1364/AO.32.004652.

Mishchenko, M. I. (2000), Calculation of the amplitude matrix for a nonspherical particle in a fixed orientation, *Appl. Opt.*, *39*(6), 1026–1031, doi:10.1364/AO.39.001026.

Mishchenko, M. I., and L. D. Travis (1998), Capabilities and limitations of a current FORTRAN implementation of the T-matrix method for randomly oriented, rotationally symmetric scatterers, *J. Quant. Spectrosc. Radiat. Transf.*, *60*(3), 309–324, doi:10.1016/S0022-4073(98)00008-9.

Mishchenko, M. I., L. D. Travis, and D. W. Mackowski (1996), T-matrix computations of light scattering by nonspherical particles: A review, *J. Quant. Spectrosc. Radiat. Transf.*, *55*(5), 535–575, doi:10.1016/0022-4073(96)00002-7.

Mishchenko, M. I., L. D. Travis, and A. A. Lacis (2005), *Scattering, Absorption and Emission of Light by Small Particles*, 448 pp., Cambridge Univ. Press, New York.

Nieminen, T., H. Rubinsztein-Dunlop, and N. Heckenberg (2003), Calculation of the T-matrix: General considerations and application of the point-matching method, *J. Quant. Spectrosc. Radiat. Transf.*, *79–80*, 1019–1029, doi:10.1016/S0022-4073(02)00336-9.

Oguchi, T. (1981), Scattering from hydrometeors: A survey, *Radio Sci.*, *16*(5), 691–730, doi:10.1029/RS016i005p00691.

Shen, X., Y. Hong, Q. Qin, S. Chen, and T. Grout (2010), A backscattering enhanced microwave canopy scattering model based on MIMICS, Abstract H33K-06 presented at 2010 Fall Meeting, AGU, San Francisco, Calif., 13–17 Dec.

Stratton, J. A. (1941), *Electromagnetic Theory*, McGraw-Hill, New York.

Tsang, L., M. Kubacsi, and J. Kong (1981), Radiative transfer theory for active remote sensing of a layer of small ellipsoidal scatterers, *Radio Sci.*, *16*(3), 321–329, doi:10.1029/RS016i003p00321.

Tsang, L., C. E. Mandt, and K. H. Ding (1992), Monte Carlo simulations of the extinction rate of dense media with randomly distributed dielectric spheres based on solution of Maxwell's equations, *Opt. Lett.*, *17*(5), 314–316, doi:10.1364/OL.17.000314.

Tsang, L., J. A. Kong, and K. H. Ding (2000), *Scattering of Electromagnetic Waves: Theories and Applications*, John Wiley, New York.

Tsang, L., J. A. Kong, K. H. Ding, and C. O. Ao (2001), *Scattering of Electromagnetic Waves: Advanced Topics*, John Wiley, New York.

Ufimtsev, P. Y. (1957), Approximate computation of the diffraction of plane electromagnetic waves at certain metal bodies, *Sov. Phys. Tech. Phys., Engl. Transl.*, *2*(8), 1708–1718.

Ulaby, F. T., R. K. Moore, and A. K. Fung (1986), *Microwave Remote Sensing: Active and Passive*, Artech House, London.

Ulaby, F. T., K. Sarabandi, K. McDonald, M. Whitt, and M. C. Dobson (1987), Michigan Microwave Canopy Scattering Model (MIMICS), *Tech. Rep. RL022574-T-1*, Rad. Lab., Univ. of Mich., Ann Arbor.

Wang, Y. M., and W. C. Chew (1992), Accelerating the iterative inverse scattering algorithms by using the fast recursive aggregate T-Matrix algorithm, *Radio Sci.*, *27*(2), 109–116, doi:10.1029/91RS02633.

Wang, Y. M., and W. C. Chew (1993), A recursive T-Matrix approach for the solution of electromagnetic scattering by many spheres, *IEEE Trans. Antennas Propag.*, *41*(12), 1633–1639, doi:10.1109/8.273306.

Waterman, P. C. (1965), Matrix formulation of electromagnetic scattering, *Proc. IEEE*, *53*(8), 805, doi:10.1109/PROC.1965.4058.

Yan, W. Z., Y. Du, Z. Li, E. X. Chen, and J. C. Shi (2009), Characterization of the validity region of the extended T-matrix method for scattering from dielectric cylinders with finite length, *Prog. Electromagn. Res.*, *96*, 309–328, doi:10.2528/PIER09083101.

Yee, K. (1966), Numerical solution of initial boundary value problems involving Maxwell's equations in isotropic media, *IEEE Trans. Antennas Propag.*, *14*(3), 302–307, doi:10.1109/TAP.1966.1138693.

Zhang, G., L. Tsang, and Z. Chen (1996), Collective scattering effects of trees generated by stochastic Lindenmayer systems, *Microwave Opt. Technol. Lett.*, *11*(2), 107–111, doi:10.1002/(SICI)1098-2760(19960205)11:2<107::AID-MOP18>3.0.CO;2-B.